Blood First Edition Paper, prepublished online January 19, 2017; DOI 10.1182/blood-2016-09-736892

Identification of apilimod as a first-in-class PIKfyve kinase inhibitor for treatment of B-cell non-Hodgkin lymphoma

Running Title: PIKFYVE Inhibitor for B-Cell Non-Hodgkin Lymphoma

Authors: Sophia Gayle[1,2], Sean Landrette[1,2], Neil Beeharry[1,2], Chris Conrad[2], Marylens Hernandez[2], Paul Beckett[2], Shawn M. Ferguson[3], Talya Mandelkern[2], Meiling Zheng[4], Tian Xu[5], Jonathan Rothberg[2] and Henri Lichenstein[2*]

[1]**Shared First Authorship**: S.G., S.L. and N.B. contributed equally to this work.

Affiliations:

[2]LAM Therapeutics, 530 Whitfield St., Guilford CT 06437

[3]Department of Cell Biology, Program in Cellular Neuroscience, Neurodegeneration and Repair, Yale University School of Medicine, New Haven CT, O6510, USA.

[4]Department of Cancer Pharmacology, CrownBioscience Inc. Changping Sector of Zhongguancun Scientific Park, No.21 Huoju Road, Changping District, Beijing, 102200, P.R. China.

[5]Howard Hughes Medical Institute, Department of Genetics, Yale University School of Medicine, 295 Congress Avenue, New Haven, Connecticut 06519, USA.

*Corresponding author. E-mail: hlichens@lamthera.com

Phone: 203-458-7100 x318 Fax: 203-458-2514

Key Points

- Apilimod has broad anti-cancer activity *in vitro* and *in vivo* across all subtypes of B-NHL
- Apilimod induces B-NHL cytotoxicity through a unique mechanism of action that involves the disruption of lysosomal function

Abstract

We identified apilimod as an anti-proliferative compound by high-throughput screening of clinical stage drugs. Apilimod exhibits exquisite specificity for PIKfyve lipid kinase and has selective cytotoxic activity in B-cell non-Hodgkin lymphoma (B-NHL) compared to normal cells. Apilimod displays nanomolar activity *in vitro,* and *in vivo* studies demonstrate single agent efficacy as well as synergy with approved B-NHL drugs. Using biochemical and knockdown approaches, and discovery of a kinase domain mutation conferring resistance, we demonstrate that apilimod-mediated cytotoxicity is driven by PIKfyve inhibition. Furthermore, a critical role for lysosome dysfunction as a major factor contributing to apilimod's cytotoxicity is supported by a genome-wide CRISPR screen. In the screen, TFEB (master transcriptional regulator of lysosomal biogenesis), and endosomal/lysosomal genes *CLCN7, OSTM1*, and *SNX10* were identified as important determinants of apilimod sensitivity. These findings thus suggest that disruption of lysosomal homeostasis with apilimod represents a novel approach to treat B-NHL.

Introduction

Non-Hodgkin lymphoma (NHL) is a collective term for a heterogeneous group of lymphoproliferative malignancies with subtypes ranging from slow-growing to aggressive with different responses to available treatment. In 2015, there were 71,850 estimated new cases of NHL and 19,790 resulting deaths [1]. Current treatment modalities for B-cell NHL (B-NHL) may be effective in first line therapy, but many patients relapse or are refractory, necessitating the development of improved therapies [2,3].

We identified apilimod from our clinical stage compound library as a potent targeted agent with robust cytotoxic activity on B-NHL. Apilimod was previously identified as an inhibitor of toll-like receptor (TLR)-induced IL-12 and IL-23 cytokine production, and was evaluated in clinical trials as an immunomodulatory agent for treatment of Th1- and Th17-mediated inflammatory diseases [4,5]. These trials included normal healthy volunteers (Phase 1) as well as psoriasis, rheumatoid arthritis, and Crohn's disease patients (Phase 2) [4,6,7]. Altogether, greater than 700 subjects were treated and apilimod was well-tolerated with mild to moderate side effects including headache, fatigue, dizziness and nausea. However, apilimod did not meet the primary endpoints in Phase 2 inflammatory disease indications and further clinical development was abandoned [4,6].

While these clinical trials were performed prior to identification of the direct target, inhibition of phosphatidylinositol-3-phosphate 5-kinase (PIKfyve) has since been shown to underlie the selective inhibition of immune cell production of IL-12/IL-23 [8]. PIKfyve is an endosomal lipid kinase targeted to the cytoplasmic leaflet of endosomes via protein-lipid interactions between its FYVE domain and phosphatidylinositol-3-

phosphate within the endosomal membrane [9]. At endosomes, PIKfyve phosphorylates PI3P to generate $PI(3,5)P_2$, which in turn serves to control endolysosomal membrane traffic [10-14].

A role for PIKfyve inhibition for anti-cancer therapy has only been minimally explored. Anti-proliferative activity of apilimod to date has been limited to experiments on non-small cell lung cancer lines [15] and under nutrient starvation [16]. A role for PIKfyve in controlling tumor cell invasiveness has also been described [17,18]. Here, we validate PIKfyve kinase as a target for B-NHL and show that inhibition by apilimod has powerful and selective anti-proliferative and cytotoxic effects. Furthermore, through a genome-wide CRISPR screen we identified lysosome-related genes that determine the remarkable sensitivity of B-NHL cells to apilimod. These findings, along with observations that apilimod treatment robustly impairs endolysosomal membrane traffic, point to disruption of lysosomal homeostasis as an important component of the cytotoxic effects of apilimod. Collectively, these findings provide a promising new approach for treating multiple subtypes of B-NHL as a single agent, or in combination with existing therapies.

Methods

Cell-Titer Glo™ Assays

Cells were seeded into 96-well plates at a density within log growth phase and treated with indicated drugs for 5 days. Plates were developed with Cell-Titer Glo™ assay (Promega) according to the manufacturer's instructions. The IC_{50} for each cell line was determined using Graphpad Prism 6 ™ software. Data were log transformed and subjected to non-linear regression (curve fit) using the sigmoidal dose-response (variable

slope) equation, constraining the bottom at 0 and the top at 100. Experiments were performed in duplicate and repeated a minimum of two independent times to obtain the average IC_{50} values. For Caspase 3/7 activity, the same procedure was performed with the Caspase Glo^{TM} assay (Promega).

Knockdown Experiments

shRNA-mediated knockdown was performed by cloning annealed hairpin oligos into Tet-pLKO-puro (Addgene plasmid 21915) for doxycycline inducible repression of *PIKFYVE* (see Supplement). Constructs were transfected into 293T cells with pVSVG and Delta 8.9 packaging plasmids and lentivirus-containing supernatant was harvested 72 hours post transfection. B-NHL cell lines were transduced by spinoculation with 50% virus supernatant with 8 ug/ml polybrene for 1.5 hours at 800 x g and drug-selected with 2 ug/ml puromycin. Surviving Tet-pLKO-puro pools were expanded and treated with 1-2 ug/mL doxycycline to induce hairpin expression.

Cell Line Transfections and Overexpression

Human *PIKFYVE, CTSD* and *TFEB* cDNAs were amplified using Kapa HiFi (Kapa Biosystems) and cloned into the piggyBac transposon construct PJ[puro] [19] Mlu I site using NEBuilder HiFi Assembly Mix (New England Biolabs). Five million cells were electroporated with a 2:1 ratio of PJ[puro] and ACT-PBase with the Neon transfection system (ThermoFisher Scientific). Pools were selected for one week with 2 ug/mL puromycin.

Xenograft Experiments

All animal studies were conducted under approved animal care protocols and AAALAC standards. Cells were propagated as described in the supplement for each specific model. Six to eight week old female mice were γ-irradiated 24 hours before tumor cell inoculation and were dosed as described in the supplement. Mice that had an adverse event before drug treatment completion were removed from the data set. See Supplement for specific details.

FACS Analysis

Cells were labelled with 7-AAD (BD Biosciences), Annexin V (BD Biosciences) or LysoTracker Deep Red (ThermoFisher Scientific) according to the manufacturers' recommendations and analyzed on a BD LSRII (BD Biosciences).

Global Gene Expression Analysis

SU-DHL-10 and WSU-DLCL2 cell lines were treated with apilimod (300 nM) or vehicle for 24 hours. RNA was isolated from three biological replicates using the RNeasy Kit (Qiagen). 100 ng of RNA was amplified using the Ion AmpliSeq Transcriptome Human Gene Expression kit (Ion AmpliSeq Transcriptome Human Gene Expression Kit, ThermoFisher) prior to Proton sequencing (Proton, ThermoFisher). Reads were demultiplexed and aligned to the reference library using the AmpliSeq RNA plug-in on the Ion Torrent Server. The differential expression between treated and control samples was determined using the DESeq2 library [20] from R Bioconductor software [21] (http://www.bioconductor.org). Statistical significance was established by calculation of

the false discovery rate (FDR) and genes with FDR < 0.05 were considered differentially regulated.

Gene Ontology Analysis

Gene ontology analysis was performed on the commonly up-regulated and down-regulated genes, using the Enrichr platform [22], and 'GO Cellular Component' term.

CRISPR screen

The dual vector lentiviral GeCKO V2 human library [23] was used to perform a genetic screen to identify genes that are required for apilimod sensitivity in the SU-DHL-10 DLBCL cell line. Four independent pools were screened at three concentrations of apilimod: 0 nM, 300 nM, and 600 nM. See Supplement for full details.

Results

High-throughput screen of clinical stage drug library identifies apilimod as a highly potent anti-proliferative drug

We compiled a unique clinical stage compound library consisting of virtually all FDA-approved small molecule drugs (i.e. 1,994 unique chemical structures) and 499 unapproved drugs that span a wide range of diseases. To systematically probe our library for drugs with anti-proliferative activity, we developed a high-throughput screening assay using a *Tsc2* null murine embryonic fibroblast (MEF) cell line displaying constitutively elevated mTORC1 signaling [24]. Apilimod was identified among the most potent drugs screened and was subsequently shown to have an IC_{50} of 20 nM (Figures S1A and S1B).

B-NHL cells display acute sensitivity to apilimod *in vitro*

Given the potency of apilimod in our initial screen, we next profiled its anti-proliferative activity against 146 cell lines representing eleven tumor types. While cells from many cancer lineages responded to apilimod, we observed that B-NHL lines were the most broadly sensitive (Figure S2). We noted anti-proliferative activity in all B-NHL subtypes with approximately 73% of lines having an IC_{50} less than 200 nM (Fig. 1A) and defined these as sensitive. Notably, significant anti-proliferative activity was observed on cell lines derived from difficult to treat double and triple hit B-NHL. Although we initially identified apilimod through screening of an mTORC1 hyper-activated cell line, we observed potent anti-proliferative activity in B-NHL lines irrespective of mTORC1 activation (Table S1 and Figure S3). Furthermore, apilimod did not affect mTORC1 signaling (Figure S3B). Overall, apilimod had selective anti-proliferative activity for B-NHL compared to normal cells with IC_{50} of 142 nM and 12,782 nM, respectively (Figure 1B and 1C; see Tables S1 and S2 for cell line specific data in lymphoma and normal cells).

Validation of PIKfyve kinase as the target responsible for anti-proliferative activity of apilimod in B-NHL

In immune cells, apilimod was previously shown to target the endosomal lipid kinase PIKfyve through direct inhibition of its kinase activity [8]. To determine if PIKfyve is also the critical target of apilimod in cancer cells, we employed chemical capture mass spectrometry (CCMS; [25]). This strategy identified two proteins as high probability apilimod targets: PIKfyve and its binding partner, VAC14 [26], (Figure S4A). Dissociation

constant (K_d) analysis with a sensitive qPCR readout demonstrated that apilimod had high affinity for PIKfyve, with K_d of 75 pM (Figure S4B and Supplemental Methods), contrasted to the previously reported K_d of 65 nM identified with a different technology [8]. To perform a comprehensive analysis of selectivity, we profiled apilimod at 1 uM against a panel of 456 normal and disease-related protein and lipid kinases [27]. The results from this screen showed that apilimod only bound to PIKfyve and not to any other kinase in the panel, including other structurally related lipid kinases such as Type I and Type II PIP5K (Figure S4C). These data confirmed and extended previous analyses showing that apilimod had selectivity for PIKfyve when profiled against 41, or 276 kinases [8,28].

We next confirmed that suppression of *PIKFYVE* levels via inducible expression of shRNAs is sufficient to inhibit the proliferation of B-NHL *in vitro* (Figure 1D and Figure S5). Furthermore, we identified through *in vitro* selection (21 days, 500 nM apilimod), a missense mutation in *PIKFYVE* that conferred apilimod resistance in the WSU-DLCL2 cell line. This N1939K mutation is predicted to reside in the ATP-binding pocket of the PIKfyve kinase domain [28]. Stable expression of the N1939K mutant conferred greater than 150-fold drug resistance as compared to the parental WSU-DLCL2 line (Figure 1E), confirming that PIKfyve is the critical target responsible for anti-proliferative activity of apilimod in B-NHL.

Apilimod displays anti-tumor activity in B-NHL *in vivo*

We next tested the effects of apilimod in *in vivo* models of lymphoma. The *in vivo* activity of apilimod was first validated in a subcutaneous Daudi Burkitt's lymphoma xenograft model. Dose dependent (50 - 150 mg/kg free base; once a day) tumor growth

inhibition was noted and no significant effect on body weight was observed (Figure 2A). In order to test if apilimod had synergistic activity *in vivo* when combined with an immunological treatment, we used a mouse strain capable of natural killer (NK) cell antibody-dependent cellular cytotoxicity (ADCC). With oral dosing of 60 mg/kg apilimod dimesylate (~41 mg/kg apilimod free base; twice a day), we observed 48% tumor growth inhibition in the SU-DHL-6 model. Single agent rituximab had 58% growth inhibition and synergy was noted for the combination with 83% tumor growth inhibition (Figure 2B). Further evaluation of apilimod in an immunocompetent A20 syngeneic lymphoma model provided the opportunity to investigate apilimod in combination with the immuno-oncology therapeutic, anti-PD-L1. Apilimod showed significant synergism in the A20 model manifesting as 86% tumor growth inhibition for the combination with anti-PD-L1, compared with 51% and 53% in the apilimod and anti-PD-L1 single arms, respectively (Figure 2C). Importantly, apilimod serum concentrations achieved in xenograft studies and in completed or ongoing clinical trials exceed concentrations known to be cytotoxic in B-NHL cellular assays (unpublished clinical data from previous Sponsor and LAM Therapeutics).

Apilimod-induced cell death in B-NHL correlates with autophagy dysfunction

To determine whether apilimod induced cytotoxicity in cancer cells, we co-stained B-NHL with Annexin V, a marker for early apoptosis, and 7-AAD, a membrane impermeant marker of nonviable cells. We observed a marked loss of membrane integrity and increased Annexin V staining in apilimod-treated B-NHL, confirming induction of cell death (Figure 3A and Figure S6A). Although Annexin V staining could be indicative

of early apoptosis, the precise mechanism of apilimod-induced cell death appears to be non-canonical. We do not observe marked increases in DEVD-UltraGlo™ Luciferase cleavage (surrogate for caspase 3/7 activity) in apilimod-treated B-NHL at physiologically relevant concentrations (Figure 3B and Figure S6B), nor do we observe a significant rescue of cell viability with caspase, cathepsin or necroptosis inhibitors across the cell lines tested (Figures 3C-3E and Figure S6C-E). Interestingly, apilimod appears to disrupt the completion of autophagy as indicated by an increase in the levels of p62 and LC3-II (Figure 3F and Figure S6F). Moreover, since co-treatment with bafilomycin does not further elevate LC3-II levels, but rapamycin does (Figure 3F and Figure S6F), apilimod most likely impairs the lysosomal degradation of autophagosomal cargo. Together this data suggests that apilimod blocks autophagy and its effects are distinct from apoptosis, lysosomal membrane permeabilization, and necroptosis.

Transcription Factor EB (TFEB) confers sensitivity to apilimod in B-NHL

To further elucidate apilimod's mechanism of action, we investigated global gene expression changes after treatment of B-NHL tumor lines (Figure 4A). Gene ontology analysis revealed a significant up-regulation of lysosomal and autophagy-related genes, results that were further confirmed with Gene Set Enrichment Analysis over a comprehensive autophagy-lysosomal signature (Figure 4B and Figure S7). Consistent with these changes in gene expression, we observed an expansion of the acidified compartment following acute apilimod treatment of B-NHL cells (Figure 4C). This result suggested that lysosome biogenesis was up-regulated by apilimod. Since TFEB is a master transcriptional regulator of lysosomal gene expression and undergoes nuclear

translocation following dephosphorylation [29-31], we explored TFEB phosphorylation status and sub-cellular localization upon apilimod treatment. We observed that within two hours of apilimod treatment, TFEB is dephosphorylated (revealed by an increase in electrophoretic mobility) and translocated into the nucleus (Figure 4D), as has been observed in other cell types with apilimod [32] and *Pikfyve* deletion [33].

We next tested the potential role of TFEB for conferring sensitivity to apilimod in B-NHL. TFEB was over-expressed in the TFEB-deficient B-NHL cell line CA46 and we observed that apilimod sensitivity was enhanced by greater than 50-fold (Figure 4E and 5B). This TFEB-mediated sensitivity also correlated with an increase in the apilimod-induced expansion of the acidified compartment, consistent with a role for lysosome dysfunction in driving apilimod-induced cell death (Figure S8). To determine whether there was a correlation between *TFEB* expression and apilimod sensitivity, we analyzed the expression levels of *TFEB* across different cancer types from the Cancer Cell Line Encyclopedia (CCLE) database [34]. Strikingly, *TFEB* was expressed most highly in B-NHL compared to other tumor types (Figure 4F). These observations support the hypothesis that elevated TFEB expression levels are an important contributor to the selective sensitivity of B-NHL cell lines to apilimod.

Disruption of lysosomal homeostasis is central to apilimod's mechanism of action

Previous studies in cell types other than B-NHL have shown that the $PI(3,5)P_2$ depletion following PIKfyve inhibition or deletion results in a striking swelling of endolysosomal organelles [8,11,35,36]. We also noted this endolysosomal swelling phenotype (vacuolization) in apilimod-treated B-NHL cells (Figure 5A). This change in the shape

and size of endosomes and lysosomes suggests a major imbalance in the membrane traffic into and out of these organelles. Lysosome function is critically dependent on the vesicular delivery and maturation of numerous enzymes that collaborate within lysosomes to degrade macromolecules. Consistent with an intracellular trafficking defect, we observed a dose-dependent increase in the pro- (inactive forms) forms of cathepsins A and D that is further enhanced by elevated TFEB expression (Fig. 5B). To confirm that apilimod was indeed causing accumulation of pro-cathepsin and not simply raising cathepsin expression, we overexpressed cathepsin D and once again observed a selective increase of pro-cathepsin D levels upon apilimod treatment (Figure S9). These results collectively demonstrate that apilimod treatment impairs the maturation of key lysosomal proteases.

Genome wide CRISPR screen identifies lysosomal proteins as key determinants of apilimod-mediated sensitivity

We next used CRISPR technology to perform a genome-wide loss of function genetic screen in the SU-DHL-10 B-NHL cell line to identify genes that are necessary for apilimod sensitivity (detailed in Figure S10). For this purpose, we used the GeCKO library that has been successfully implemented in previous CRISPR-based resistance screens [23,37]. Briefly, cells were infected in parallel with the GeCKO A and B libraries and expanded in the presence of 300 nM or 600 nM apilimod. After 3 days of treatment, surviving cells were further expanded and reselected in the presence of apilimod for another 3 days. Genomic DNA from these pools was subsequently analyzed for the identification of enriched single-guide RNAs (sgRNAs).

Remarkably, the endosomal/lysosomal associated genes *OSTM1*, *CLCN7*, *SNX10*, as well as *TFEB* were top hits arising from this analysis (Figure 5C). This identification of TFEB (in addition to data from Figure 4E) further establishes this transcription factor as an important determinant of apilimod sensitivity. Interestingly, *CLCN7* is a TFEB target gene [38] and together with *OSTM1* encodes a Cl-/H+ exchanger [39] that is important for lysosome acidification [40,41]. Furthermore, sorting nexin 10 (SNX10) has previously been shown to play an important role in the control of endolysosomal membrane traffic and induces large lysosomal vacuoles when over-expressed [42]. To validate these molecular candidates, we performed targeted CRISPR-mediated deletion of *OSTM1* and *CLCN7* in B-NHL cells, and observed that loss of each gene indeed conferred >100-fold apilimod resistance (Figure 5D).

In order to elucidate the connection between TFEB and the CLCN7/OSTM1 transporter, we examined the effect of knocking out each of these components on apilimod-induced lysosomal expansion. Interestingly, loss of either chloride transporter component (CLCN7 or OSTM1), but not TFEB, blocked both apilimod-induced expansion of the acidified compartment and vacuolization (Figure 6). Importantly, apilimod sensitivity correlated with these endolysosomal phenotypes as *CLCN7* and *OSTM1* CRISPR knockout confer complete resistance and *TFEB* CRISPR knockout only provides partial resistance (Figure 5D and Figure S11). This points to TFEB activity functioning upstream or parallel to the CLCN7/OSTM1 transporter, which appears to be directly required for apilimod-induced endolysosomal disruption. Together, these results support a model where CLCN7/OSTM1 is central to the susceptibility of B-NHL to apilimod-induced killing.

Discussion

In this study we identified apilimod as a drug with potent and selective anti-cancer activity against B-NHL. To better understand how apilimod exerts its cytotoxic effect, we first sought to unambiguously identify its relevant molecular target in B-NHL cells and found it to be the phosphosinositide kinase PIKfyve, matching what was previously observed in immune cells [8]. By profiling apilimod against a human kinome library, we found a remarkable selectivity for PIKfyve over all other kinases examined. Validation that PIKfyve inhibition was directly responsible for apilimod activity was provided by PIKfyve knockdown experiments. The central role for PIKfyve as the mediator of apilimod sensitivity was further supported by our identification of a kinase domain point mutant that confers dramatic resistance. Thus, pharmacological and genetic methodologies both converge on the conclusion that PIKfyve inhibition is sufficient to inhibit proliferation and survival of B-NHL. We thus corroborated previous studies that have identified PIKfyve as the target of apilimod [8] and are the first to uncover that inhibition of PIKfyve by apilimod represents a potential therapeutic strategy for treatment of B-NHL. While apilimod has previously been investigated in some cancer cell lines, our results pertaining to B-NHL are distinct. For example, a previous study demonstrated that apilimod had anti-proliferative activity on non-small cell lung cancer lines and posited that the in vitro effect was correlated with increased expression of the IL-23 receptor [15]. We searched for a connection between expression of IL-23 receptor in sensitive versus resistant lines, but did not observe any significant correlation (data not shown). Interestingly, inhibition of PIKfyve has also been shown to inhibit cancer cell

invasion [17,18] and growth under nutrient deprivation [16], which may lead to enhanced anti-tumor activity against metastatic and nutrient-deprived tumors *in vivo*.

The precise mechanism through which apilimod exerts its selective killing activity on specific cancer cells is of great interest. Consistent with expectations arising from the established role for PIKfyve as an important regulator of endosome and lysosome function [10-13,35,36,43], our experiments have provided multiple pieces of evidence that point to apilimod's disruption of late endosome/lysosome function as being a major factor driving apilimod-induced cancer cell cytotoxicity.

First, we and others have observed that loss of PIKfyve activity results in disruption of endososome and lysosome membrane trafficking [10-13,35,36,43], as revealed by the robust formation of swollen cytoplasmic vacuoles following apilimod treatment. This massive apilimod-induced trafficking defect likely disrupts multiple aspects of lysosome function. Indeed, we observed that apilimod treatment in B-NHL impairs the degradation of autophagic cargo and blocks cathepsin maturation (Figures 3F and 5B) as has been reported for other PIKfyve inhibitors [43-45] and genetic deletion [36]. Furthermore, cathepsin inhibition does not block apilimod activity (Figure 3D), suggesting a mechanism distinct from classical lysosomal membrane permeabilization [46].

Second, we observe that apilimod increases the nuclear abundance of TFEB and induces the up-regulation of numerous lysosome and autophagy-related genes as observed for TFEB activation in other cell types [38,47,48]. Interestingly, as previously reported [32], apilimod-induced TFEB nuclear translocation is independent of mTOR inhibition (Figure S3B). We were also unable to detect a role for calcineurin which was recently shown to regulate TFEB dephosphorylation and nuclear translocation, [49]

suggesting a novel phosphatase acts downstream of PIKfyve to dephosphorylate TFEB in apilimod-treated cells (data not shown). Typically, TFEB-dependent up-regulation of genes encoding lysosomal proteins represents a powerful homeostatic mechanism for restoring lysosome function. However, we predict that enhancing lysosomal protein expression under conditions where endolysosomal membrane traffic is impaired may actually further stress tumor cells and contribute to their death.

Third, we have identified lysosomal proteins that are critical for apilimod cytotoxicity in B-NHL. B-NHL cells express high levels of *TFEB* compared to other tumor types and increasing *TFEB* in the *TFEB*-deficient CA46 B-NHL cell line conferred a dramatic increase in apilimod sensitivity. This important role for TFEB in apilimod-induced B-NHL cytotoxicity was also independently confirmed in our genome-wide CRISPR screen. In addition to TFEB, the lysosomal proteins CLCN7, OSTM1, and SNX10 were all required for maximal apilimod sensitivity. The fact that each of these proteins functions at late endosomes and lysosomes further support a central role for the lysosome in the cytotoxic activity of apilimod.

CLCN7 and OSTM1 form an H^+/Cl^- transporter that supports the acidification of late endosomes and lysosomes [40,41]. The dramatic apilimod resistance that arises from disrupting either of these genes points to an essential role for this ion transporter in apilimod-induced cytotoxicity. Interestingly, deletion of these genes also blocked the ability of apilimod to induce vacuole formation and expand the acidified compartment of the lysosome. Such an observation is consistent with the recent report that endolysosome acidification is critical for vacuole formation downstream of $PI(3,5)P_2$ depletion [50]. While our new observations suggest that the CLCN7/OSTM1 transporter is required for

endolysosomal trafficking defects that contribute to apilimod cytotoxicity, further studies will be required to define specific mechanisms that couple CLCN7/OSTM1 function to $PI(3,5)P_2$ availability.

Collectively, these new findings identify apilimod-mediated inhibition of PIKfyve as a promising new therapeutic strategy, and have more broadly elucidated disruption of lysosomal homeostasis as a novel anti-cancer mechanism for the killing of B-NHL tumor cells. Our experiments have revealed that apilimod disrupts multiple lysosome activities ranging from TFEB-dependent regulation of lysosomal gene expression, maturation of lysosomal proteases, endolysosomal membrane trafficking, and autophagic cargo clearance. While the relative contributions of each of these factors to the sensitivity of B-NHL cells to apilimod remain to be determined, our results parallel an increasing appreciation for the diverse roles played by lysosomes as signaling and degradative organelles with major relevance to the control of cell growth [51,52].

From a clinical perspective, apilimod meets prerequisite requirements for evaluation as a novel first-in-class kinase inhibitor to treat B-NHL. The drug has potent activity against its biochemical target leading to cytotoxicity in B-NHL, and is active in xenograft models both as single agent, as well as in combination with rituximab and anti-PD-L1. Prior to entry in human clinical trials, apilimod had been extensively tested in long-term GLP toxicology studies in mice, rats, dogs and monkeys. Furthermore, the ubiquitous expression of PIKfyve does not appear to pose toxicity issues as the pharmacokinetic and safety profiles of apilimod in greater than 700 human subjects (normal healthy volunteers and inflammatory disease patients) have been assessed. Apilimod is therefore suitable for clinical evaluation in cancer patients. To this end, in

our ongoing clinical trial (NCT02594384), we are formally defining a maximal tolerated dose (MTD) for apilimod in B-NHL patients and monitoring safety, PK/PD, and preliminary efficacy.

Acknowledgements: We thank D. Kwiatkowski for providing the MEF *Tsc2* null cell line used in this study and Southern Research Institute for performing the high-throughput screen. We thank P. De Camilli, B. Manning, J. Bader and M. Dyer for their helpful scientific discussions and review of this manuscript. We also thank L. Melvin and J. Abramson for their insight and review of this manuscript. S.G., N.B., S.L., C.C., P.B., M.H., T.M. and H.L. are employees at LAM Therapeutics. T.X. is on the advisory board, S.M.F. is consultant to LAM. M.Z. works for Crown Biosciences, a contract research organization used by LAM, and J.R. is a Director of LAM Therapeutics.

Author contributions: H.L. and J.R. conceived and directed the project and S.G., N.B., S.L., and C.C. designed and conducted the experiments. P.B. curated the compound library and directed library screening. M.H. performed the bioinformatics analyses. T.M. conducted the expression analysis experiments. M.Z. conducted the xenograft model experiments. H.L., T.X., S.M.F., and J.R. provided major intellectual input for the project design. S.G., S.L., N.B. and H.L. wrote the manuscript and C.C., S.M.F., M.H. and P.B. contributed to the writing of the manuscript.

Conflict-of-interest disclosure: S.G., N.B., S.L., C.C., P.B., M.H., T.M. and H.L. are employees at LAM Therapeutics. T.X. is on the advisory board, S.M.F. is a consultant to LAM. M.Z. works for Crown Biosciences, a contract research organization used by LAM, and J.R. is a Director of LAM Therapeutics. LAM Therapeutics is the owner of apilimod patents. This study was sponsored by LAM Therapeutics.

Data and materials availability: The MEF *Tsc2* null cell line was obtained from the Kwiatkowski lab. All other normal and cancer cell lines used are commercially available from ATCC or DSMZ and identification verified by these organizations through STR profiling.

Funding: This study was sponsored by LAM Therapeutics.

References:

1. SEER Program (www.seer.cancer.gov) SEER*Stat Database: Mortality - All COD AWS, Total U.S. (1969-2012 <Katrina/Rita Population Adjustment>, National Cancer Institute, DCCPS, Surveillance Research Program, Surveillance Systems Branch. SEER Stat Fact Sheets: Non-Hodgkin Lymphoma. Bethseda, MD; 2015.

2. Alexander DD, Mink PJ, Adami HO, et al. The non-Hodgkin lymphomas: a review of the epidemiologic literature. *Int J Cancer*. 2007;120 Suppl 12:1-39.

3. Elis A, Blickstein D, Klein O, Eliav-Ronen R, Manor Y, Lishner M. Detection of relapse in non-Hodgkin's lymphoma: role of routine follow-up studies. *Am J Hematol*. 2002;69(1):41-44.

4. Krausz S, Boumans MJ, Gerlag DM, et al. Brief report: a phase IIa, randomized, double-blind, placebo-controlled trial of apilimod mesylate, an interleukin-12/interleukin-23 inhibitor, in patients with rheumatoid arthritis. *Arthritis Rheum*. 2012;64(6):1750-1755.

5. Wada Y, Lu R, Zhou D, et al. Selective abrogation of Th1 response by STA-5326, a potent IL-12/IL-23 inhibitor. *Blood*. 2007;109(3):1156-1164.

6. Sands BE, Jacobson EW, Sylwestrowicz T, et al. Randomized, double-blind, placebo-controlled trial of the oral interleukin-12/23 inhibitor apilimod mesylate for treatment of active Crohn's disease. *Inflamm Bowel Dis*. 2010;16(7):1209-1218.

7. Wada Y, Cardinale I, Khatcherian A, et al. Apilimod inhibits the production of IL-12 and IL-23 and reduces dendritic cell infiltration in psoriasis. *PLoS One*. 2012;7(4):e35069.

8. Cai X, Xu Y, Cheung AK, et al. PIKfyve, a class III PI kinase, is the target of the small molecular IL-12/IL-23 inhibitor apilimod and a player in Toll-like receptor signaling. *Chem Biol*. 2013;20(7):912-921.

9. Sbrissa D, Ikonomov OC, Shisheva A. Phosphatidylinositol 3-phosphate-interacting domains in PIKfyve. Binding specificity and role in PIKfyve. Endomenbrane localization. *J Biol Chem.* 2002;277(8):6073-6079.

10. de Lartigue J, Polson H, Feldman M, et al. PIKfyve regulation of endosome-linked pathways. *Traffic*. 2009;10(7):883-893.

11. Ikonomov OC, Sbrissa D, Mlak K, Kanzaki M, Pessin J, Shisheva A. Functional dissection of lipid and protein kinase signals of PIKfyve reveals the role of PtdIns 3,5-P2 production for endomembrane integrity. *J Biol Chem*. 2002;277(11):9206-9211.

12. Ikonomov OC, Sbrissa D, Shisheva A. Mammalian cell morphology and endocytic membrane homeostasis require enzymatically active phosphoinositide 5-kinase PIKfyve. *J Biol Chem.* 2001;276(28):26141-26147.

13. Rutherford AC, Traer C, Wassmer T, et al. The mammalian phosphatidylinositol 3-phosphate 5-kinase (PIKfyve) regulates endosome-to-TGN retrograde transport. *J Cell Sci*. 2006;119(Pt 19):3944-3957.

14. Zolov SN, Bridges D, Zhang Y, et al. In vivo, Pikfyve generates PI(3,5)P2, which serves as both a signaling lipid and the major precursor for PI5P. *Proc Natl Acad Sci U S A*. 2012;109(43):17472-17477.

15. Baird AM, Dockry E, Daly A, et al. IL-23R is Epigenetically Regulated and Modulated by Chemotherapy in Non-Small Cell Lung Cancer. *Front Oncol*. 2013;3:162.

16. Krishna S, Palm W, Lee Y, et al. PIKfyve Regulates Vacuole Maturation and Nutrient Recovery following Engulfment. *Dev Cell*. 2016;38(5):536-547.

17. Dupuis-Coronas S, Lagarrigue F, Ramel D, et al. The nucleophosmin-anaplastic lymphoma kinase oncogene interacts, activates, and uses the kinase PIKfyve to increase invasiveness. *J Biol Chem*. 2011;286(37):32105-32114.

18. Oppelt A, Haugsten EM, Zech T, et al. PIKfyve, MTMR3 and their product PtdIns5P regulate cancer cell migration and invasion through activation of Rac1. *Biochem J*. 2014;461(3):383-390.

19. Gayle S, Pan Y, Landrette S, Xu T. piggyBac insertional mutagenesis screen identifies a role for nuclear RHOA in human ES cell differentiation. *Stem Cell Reports*. 2015;4(5):926-938.

20. Love MI, Huber W, Anders S. Moderated estimation of fold change and dispersion for RNA-seq data with DESeq2. *Genome Biol*. 2014;15(12):550.

21. Gentleman RC, Carey VJ, Bates DM, et al. Bioconductor: open software development for computational biology and bioinformatics. *Genome Biol*. 2004;5(10):R80.

22. Chen EY, Tan CM, Kou Y, et al. Enrichr: interactive and collaborative HTML5 gene list enrichment analysis tool. *BMC Bioinformatics*. 2013;14:128.

23. Sanjana NE, Shalem O, Zhang F. Improved vectors and genome-wide libraries for CRISPR screening. *Nat Methods*. 2014;11(8):783-784.

24. Huang J, Dibble CC, Matsuzaki M, Manning BD. The TSC1-TSC2 complex is required for proper activation of mTOR complex 2. *Mol Cell Biol*. 2008;28(12):4104-4115.

25. Koster H, Little DP, Luan P, et al. Capture compound mass spectrometry: a technology for the investigation of small molecule protein interactions. *Assay Drug Dev Technol*. 2007;5(3):381-390.

26. Botelho RJ, Efe JA, Teis D, Emr SD. Assembly of a Fab1 phosphoinositide kinase signaling complex requires the Fig4 phosphoinositide phosphatase. *Mol Biol Cell*. 2008;19(10):4273-4286.

27. Davis MI, Hunt JP, Herrgard S, et al. Comprehensive analysis of kinase inhibitor selectivity. *Nat Biotechnol*. 2011;29(11):1046-1051.

28. Hayakawa N, Noguchi M, Takeshita S, et al. Structure-activity relationship study, target identification, and pharmacological characterization of a small molecular IL-12/23 inhibitor, APY0201. *Bioorg Med Chem*. 2014;22(11):3021-3029.

29. Settembre C, Zoncu R, Medina DL, et al. A lysosome-to-nucleus signalling mechanism senses and regulates the lysosome via mTOR and TFEB. *EMBO J*. 2012;31(5):1095-1108.

30. Roczniak-Ferguson A, Petit CS, Froehlich F, et al. The transcription factor TFEB links mTORC1 signaling to transcriptional control of lysosome homeostasis. *Sci Signal*. 2012;5(228):ra42.

31. Martina JA, Chen Y, Gucek M, Puertollano R. MTORC1 functions as a transcriptional regulator of autophagy by preventing nuclear transport of TFEB. *Autophagy*. 2012;8(6):903-914.

32. Wang W, Gao Q, Yang M, et al. Up-regulation of lysosomal TRPML1 channels is essential for lysosomal adaptation to nutrient starvation. *Proc Natl Acad Sci U S A*. 2015;112(11):E1373-1381.

33. Min SH, Suzuki A, Guzman J, Abrams CS. Pikfyve is essential for lysosomal homeostasis in macrophages. Annual Meeting of the American Society of Hematology. Vol. 124 no. 21 461. San Francisco CA: Blood; 2014.

34. Barretina J, Caponigro G, Stransky N, et al. The Cancer Cell Line Encyclopedia enables predictive modelling of anticancer drug sensitivity. *Nature*. 2012;483(7391):603-607.

35. Dong XP, Shen D, Wang X, et al. PI(3,5)P(2) controls membrane trafficking by direct activation of mucolipin Ca(2+) release channels in the endolysosome. *Nat Commun*. 2010;1:38.

36. Min SH, Suzuki A, Stalker TJ, et al. Loss of PIKfyve in platelets causes a lysosomal disease leading to inflammation and thrombosis in mice. *Nat Commun*. 2014;5:4691.

37. Shalem O, Sanjana NE, Hartenian E, et al. Genome-scale CRISPR-Cas9 knockout screening in human cells. *Science*. 2014;343(6166):84-87.

38. Sardiello M, Palmieri M, di Ronza A, et al. A gene network regulating lysosomal biogenesis and function. *Science*. 2009;325(5939):473-477.

39. Leisle L, Ludwig CF, Wagner FA, Jentsch TJ, Stauber T. ClC-7 is a slowly voltage-gated 2Cl(-)/1H(+)-exchanger and requires Ostm1 for transport activity. *EMBO J*. 2011;30(11):2140-2152.

40. Graves AR, Curran PK, Smith CL, Mindell JA. The Cl-/H+ antiporter ClC-7 is the primary chloride permeation pathway in lysosomes. *Nature*. 2008;453(7196):788-792.

41. Ishida Y, Nayak S, Mindell JA, Grabe M. A model of lysosomal pH regulation. *J Gen Physiol*. 2013;141(6):705-720.

42. Qin B, He M, Chen X, Pei D. Sorting nexin 10 induces giant vacuoles in mammalian cells. *J Biol Chem*. 2006;281(48):36891-36896.

43. Kim GH, Dayam RM, Prashar A, Terebiznik M, Botelho RJ. PIKfyve inhibition interferes with phagosome and endosome maturation in macrophages. *Traffic*. 2014;15(10):1143-1163.

44. Sano O, Kazetani K, Funata M, Fukuda Y, Matsui J, Iwata H. Vacuolin-1 inhibits autophagy by impairing lysosomal maturation via PIKfyve inhibition. *FEBS Lett*. 2016;590(11):1576-1585.

45. Vicinanza M, Korolchuk VI, Ashkenazi A, et al. PI(5)P regulates autophagosome biogenesis. *Mol Cell*. 2015;57(2):219-234.

46. Boya P, Kroemer G. Lysosomal membrane permeabilization in cell death. *Oncogene*. 2008;27(50):6434-6451.

47. Perera RM, Stoykova S, Nicolay BN, et al. Transcriptional control of autophagy-lysosome function drives pancreatic cancer metabolism. *Nature*. 2015;524(7565):361-365.

48. Settembre C, Di Malta C, Polito VA, et al. TFEB links autophagy to lysosomal biogenesis. *Science*. 2011;332(6036):1429-1433.

49. Medina DL, Di Paola S, Peluso I, et al. Lysosomal calcium signalling regulates autophagy through calcineurin and TFEB. *Nat Cell Biol*. 2015;17(3):288-299.

50. Compton LM, Ikonomov OC, Sbrissa D, Garg P, Shisheva A. Active vacuolar H+ATPase and functional cycle of Rab5 are required for the vacuolation defect triggered by PtdIns(3,5)P2 loss under PIKfyve or Vps34 deficiency. *Am J Physiol Cell Physiol*. 2016:ajpcell 00104 02016.

51. Settembre C, Fraldi A, Medina DL, Ballabio A. Signals from the lysosome: a control centre for cellular clearance and energy metabolism. *Nat Rev Mol Cell Biol*. 2013;14(5):283-296.

52. Ferguson SM. Beyond indigestion: emerging roles for lysosome-based signaling in human disease. *Curr Opin Cell Biol*. 2015;35:59-68.

Figure Legends

Figure 1. B-NHL cells display acute sensitivity to apilimod *in vitro*.

(A) Sensitivity of 48 human B-NHL lines to apilimod, with sensitivity defined as an IC_{50} less than 200 nM in a 5-day Cell-Titer Glo^{TM} assay. The number of cell lines screened is indicated in parenthesis.

(B) Box and whiskers plot of average IC_{50} values (geometric mean) in human B-NHL (N=48) and normal human cell lines (N=12) treated with apilimod for 5 days. Each cell line was tested a minimum of two independent times. $P<0.0001$ by unpaired two-tailed student's t-test.

(C) Representative viability curves of lymphoma cell lines in 5-day Cell-Titer Glo^{TM} assays.

(D) Viability of WSU-DLCL2 lymphoma cells after the induction of either control or *PIKFYVE* shRNA with doxycycline for five days. Values normalized to uninduced cells.

(E) A *PIKFYVE* mutation that induces a N1939K amino acid change in the kinase domain confers apilimod resistance. Ten-point dose response of WSU-DLCL2 analysis of overexpression clones [CTRL (GFP), PIKfyve WT, and N1939K] to 3-day treatment with apilimod. Data are represented as mean ± SD.

Figure 2. Apilimod displays anti-tumor activity in B-NHL *in vivo*.

(A) Growth of Daudi Burkitt's lymphoma xenograft tumors. Left: Graph of tumor size (mm^3) over time (days). Right: Graph of body weight (g) over time (days). Dose is detailed in legend, **** $P<0.0001$; compared to vehicle at last time point, one-way ANOVA, Dunnett's post-test. Pink triangles indicate the days which apilimod was dosed. N=8 mice per treatment arm. Data are represented as mean ± SEM.

(B) Apilimod displays growth inhibition in combination with rituximab in SU-DHL-6 DLBCL tumors *in vivo*. Left: Graph of tumor size (mm^3) over time (days). Right: Graph of body weight (g) over time (days). * $P<0.05$; ** $P<0.01$ compared to vehicle at last time point, one-way ANOVA, Dunnett's post-test. Coefficient of drug interaction (CDI) 0.8, CDI < 1 indicates synergism. Pink and aqua triangles indicate the days which apilimod and rituximab were dosed. N=6 mice per treatment arm. Data are represented as mean ± SEM.

(C) Apilimod causes tumor growth inhibition in combination with anti-PD-L1 in A20 syngeneic model. Left: Graph of tumor size (mm^3) over time (days). Right: Graph of body weight (g) over time (days). *** $P<0.001$, **** $P=0.0001$ compared to vehicle at last time point, one-way ANOVA, Dunnett's post-test. Coefficient of drug interaction (CDI) 0.62, CDI < 1 indicates synergism. Pink and aqua triangles indicate the days which apilimod and anti-PD-L1 were dosed. N=8 mice per treatment arm. Data are represented as mean ± SEM.

Figure 3. Apilimod induces non-canonical cytotoxicity in B-NHL.

(A) Cytotoxicity of SU-DHL-10 B-NHL treated with either DMSO or 200 nM apilimod for 3 days and stained with the viability dye 7-AAD and the apoptotic indicator Annexin V. Percentages of single and double positive cells are displayed.

(B) DEVD-UltraGlo™ Luciferase cleavage activity in SU-DHL-10 B-NHL after 2-day treatment with the indicated concentration of apilimod.

(C) Viability of SU-DHL-10 B-NHL measured under increasing concentrations of apilimod +/- 25 uM of the caspase inhibitor Z-VAD-FMK for 3 days.

(D) Viability of SU-DHL-10 B-NHL treated with apilimod and the indicated concentration of cathepsin inhibitor (cathepsin inhibitor I, E64d, CA-074 Me, or cathepsin inhibitor III) for 3 days. Apilimod was used at 156 nM in single agent and combination experiments.

(E) Viability of SU-DHL-10 B-NHL that were pretreated for 24 hours with 5 ug/mL of the necroptosis inhibitor necrostatin-1 and subsequently co-treated with 5 ug/mL necrostatin-1 and the indicated concentration of apilimod for 3 days.

(F) Representative Western blot of SU-DHL-10 B-NHL that were treated with vehicle, apilimod (200 nM), the autophagy inducer rapamycin (5 uM) or the combination of apilimod and rapamycin in the absence or presence of the autophagy inhibitor bafilomycin A1 (500 nM added for the last 8 hours) for 24 hours. Cell lysates probed with antibodies against LC3, p62 or vinculin (loading control).

Figure 4. TFEB is a mediator of apilimod sensitivity in B-NHL.

(A) Heat map representation of gene expression changes in SU-DHL-10 and WSU-DLCL2 B-NHL lines treated with 300 nM apilimod for 24 hours. Red color represents up-regulated genes while blue color represents down-regulated genes. LOG2FC = LOG2 fold change.

(B) Gene Ontology analysis of commonly up-regulated genes from Figure 4A reveals an enrichment for lysosomal associated genes.

(C) LysoTracker staining in SU-DHL-6 and SU-DHL-10 for 24 and 48 hours after treatment with 200 nM (blue) apilimod compared to DMSO treated control (red).

(D) Nuclear and cytoplasmic levels of TFEB protein assayed by immunoblotting in SU-DHL-6 cells treated with apilimod (63 nM) for 2 hours. A representative blot is shown from 2 independent experiments.

(E) Stable CA46 (*TFEB*-deficient B-NHL) pools over-expressing either GFP control or TFEB were treated with 10-point apilimod dose response for 3 days. Data are represented as mean ± SD.

(F) Box plots showing relative *TFEB* mRNA levels across tumor types, extracted from CCLE [34] with gene centric robust multi-array analysis-normalized mRNA expression data. "Lymphoma Other" includes B-cell lymphoma unspecified (8), anaplastic large cell lymphoma (5), chronic lymphocytic leukemia- small lymphocytic lymphoma (5), mantle cell lymphoma (4), mycosis fungoides-Sezary syndrome (3), peripheral T-cell lymphoma unspecified (1), T-cell large granular lymphocytic leukemia (1), and Unclassified (1). B-NHL cell lines are highlighted with red box.

Figure 5. Apilimod disrupts lysosomal homeostasis and intracellular trafficking.

(A) SU-DHL-6 cells were treated with DMSO or 63 nM apilimod for 24 hours and imaged at 40x magnification. Arrows highlight large vacuoles. Image sharpened evenly in order to highlight vacuoles present in floating lymphoma cells.

(B) Apilimod induces pro-cathepsin accumulation. Control (CTRL) TFEB-deficient or TFEB over-expressing CA46 cells were dosed with increasing amounts of apilimod (15 nM to 1000 nM) for 24 hours. Lysates were probed with the indicated antibodies. The Pro and Mature forms of cathepsins A and D are indicated. Representative blot is shown from 2 independent experiments. Unt = untreated.

(C) Mean Z-score for top 4 genes from CRISPR apilimod resistance screen.

(D) WSU-DLCL2 B-NHL pools with the indicated *OSTM1, CLCN7* or Non-Targeting (NT) sgRNA were treated with 10-point apilimod dose response for 3 days. Data are represented as mean ± SD.

Figure 6. Effect of CRISPR gene knockout on apilimod-induced lysosomal expansion.

LysoTracker staining in WSU-DLCL2 CRISPR knockout pools 2 days after treatment with 200 nM apilimod (blue) compared to DMSO-treated control (red). Three independent sgRNA pools for each gene listed on left are displayed. NT = Non-Targeting. Corresponding images of vacuole formation in the cells are displayed on the right (40x). Arrows highlight large vacuoles. Images sharpened evenly in order to highlight vacuoles present in floating lymphoma cells.

Figure 1

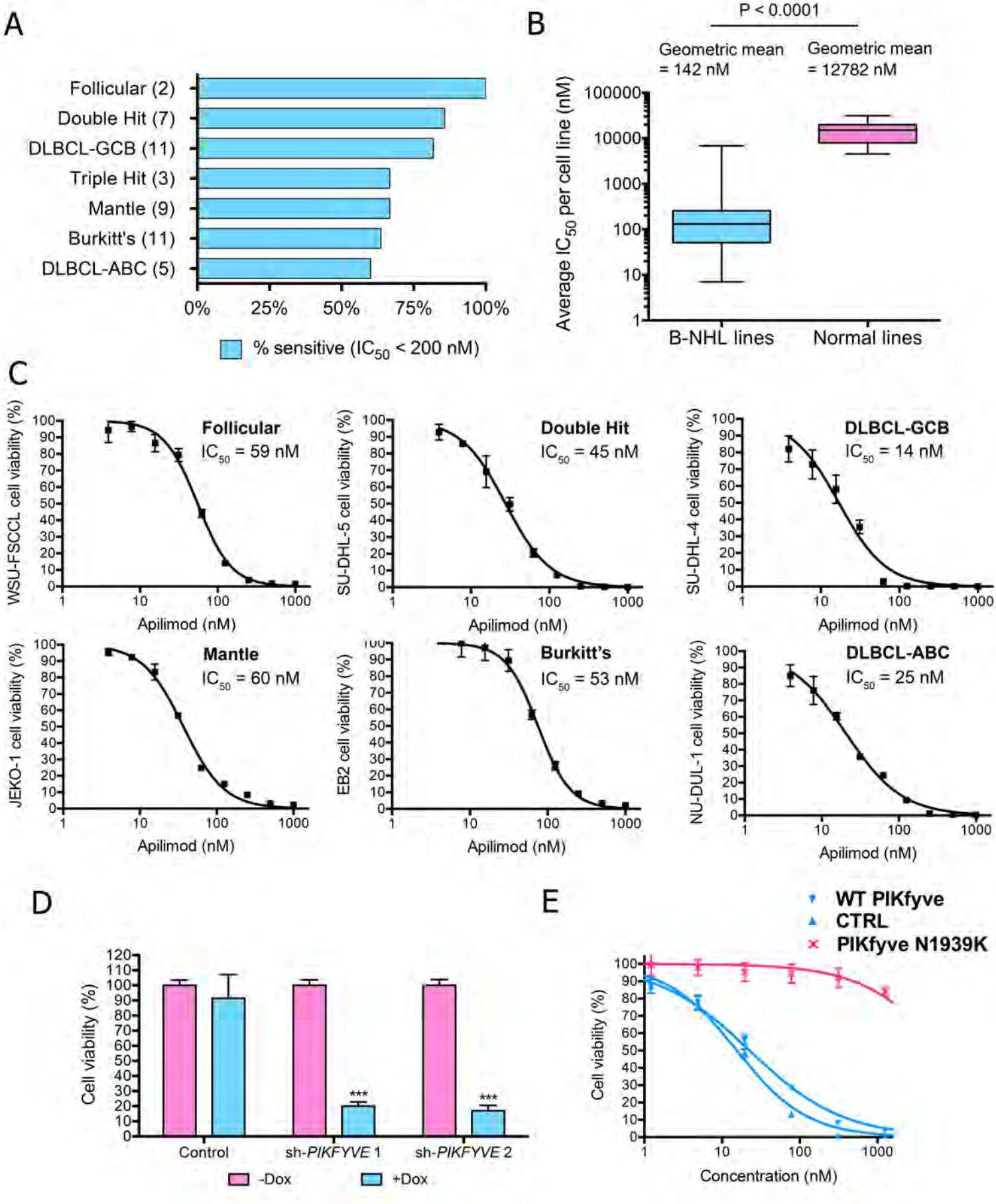
A
Follicular (2)
Double Hit (7)
DLBCL-GCB (11)
Triple Hit (3)
Mantle (9)
Burkitt's (11)
DLBCL-ABC (5)
0%
25%
50%
75%
100%
% sensitive (IC50 < 200 nM)
B
P < 0.0001
Geometric mean = 142 nM
Geometric mean = 12782 nM
Average IC50 per cell line (nM)
100000
10000
1000
100
10
1
B-NHL lines
Normal lines
C
WSU-FSCCL cell viability (%)
Follicular
IC50 = 59 nM
SU-DHL-5 cell viability (%)
Double Hit
IC50 = 45 nM
SU-DHL-4 cell viability (%)
DLBCL-GCB
IC50 = 14 nM
JEKO-1 cell viability (%)
Mantle
IC50 = 60 nM
EB2 cell viability (%)
Burkitt's
IC50 = 53 nM
NU-DUL-1 cell viability (%)
DLBCL-ABC
IC50 = 25 nM
Apilimod (nM)
D
Cell viability (%)
Control
sh-PIKFYVE 1
sh-PIKFYVE 2
***
-Dox
+Dox
E
WT PIKfyve
CTRL
PIKfyve N1939K
Cell viability (%)
Concentration (nM)

Figure 2

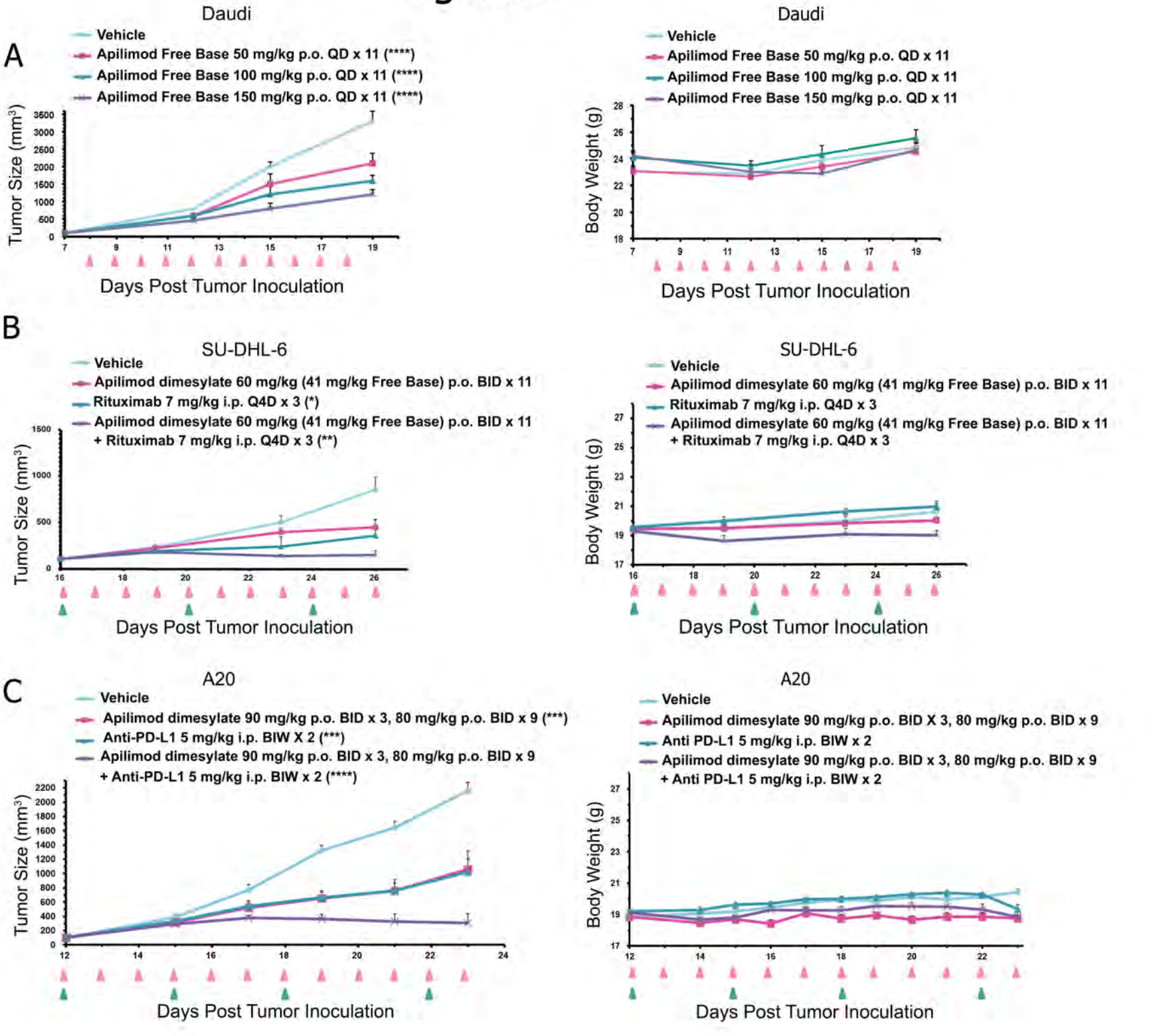
A
Daudi
Vehicle
Apilimod Free Base 50 mg/kg p.o. QD x 11 (****)
Apilimod Free Base 100 mg/kg p.o. QD x 11 (****)
Apilimod Free Base 150 mg/kg p.o. QD x 11 (****)
Tumor Size (mm3)
Days Post Tumor Inoculation
Daudi
Vehicle
Apilimod Free Base 50 mg/kg p.o. QD x 11
Apilimod Free Base 100 mg/kg p.o. QD x 11
Apilimod Free Base 150 mg/kg p.o. QD x 11
Body Weight (g)
Days Post Tumor Inoculation
B
SU-DHL-6
Vehicle
Apilimod dimesylate 60 mg/kg (41 mg/kg Free Base) p.o. BID x 11
Rituximab 7 mg/kg i.p. Q4D x 3 (*)
Apilimod dimesylate 60 mg/kg (41 mg/kg Free Base) p.o. BID x 11
+ Rituximab 7 mg/kg i.p. Q4D x 3 (**)
Tumor Size (mm3)
Days Post Tumor Inoculation
SU-DHL-6
Vehicle
Apilimod dimesylate 60 mg/kg (41 mg/kg Free Base) p.o. BID x 11
Rituximab 7 mg/kg i.p. Q4D x 3
Apilimod dimesylate 60 mg/kg (41 mg/kg Free Base) p.o. BID x 11
+ Rituximab 7 mg/kg i.p. Q4D x 3
Body Weight (g)
Days Post Tumor Inoculation
C
A20
Vehicle
Apilimod dimesylate 90 mg/kg p.o. BID x 3, 80 mg/kg p.o. BID x 9 (***)
Anti-PD-L1 5 mg/kg i.p. BIW X 2 (***)
Apilimod dimesylate 90 mg/kg p.o. BID x 3, 80 mg/kg p.o. BID x 9
+ Anti-PD-L1 5 mg/kg i.p. BIW x 2 (****)
Tumor Size (mm3)
Days Post Tumor Inoculation
A20
Vehicle
Apilimod dimesylate 90 mg/kg p.o. BID X 3, 80 mg/kg p.o. BID x 9
Anti PD-L1 5 mg/kg i.p. BIW x 2
Apilimod dimesylate 90 mg/kg p.o. BID x 3, 80 mg/kg p.o. BID x 9
+ Anti PD-L1 5 mg/kg i.p. BIW x 2
Body Weight (g)
Days Post Tumor Inoculation

Figure 3

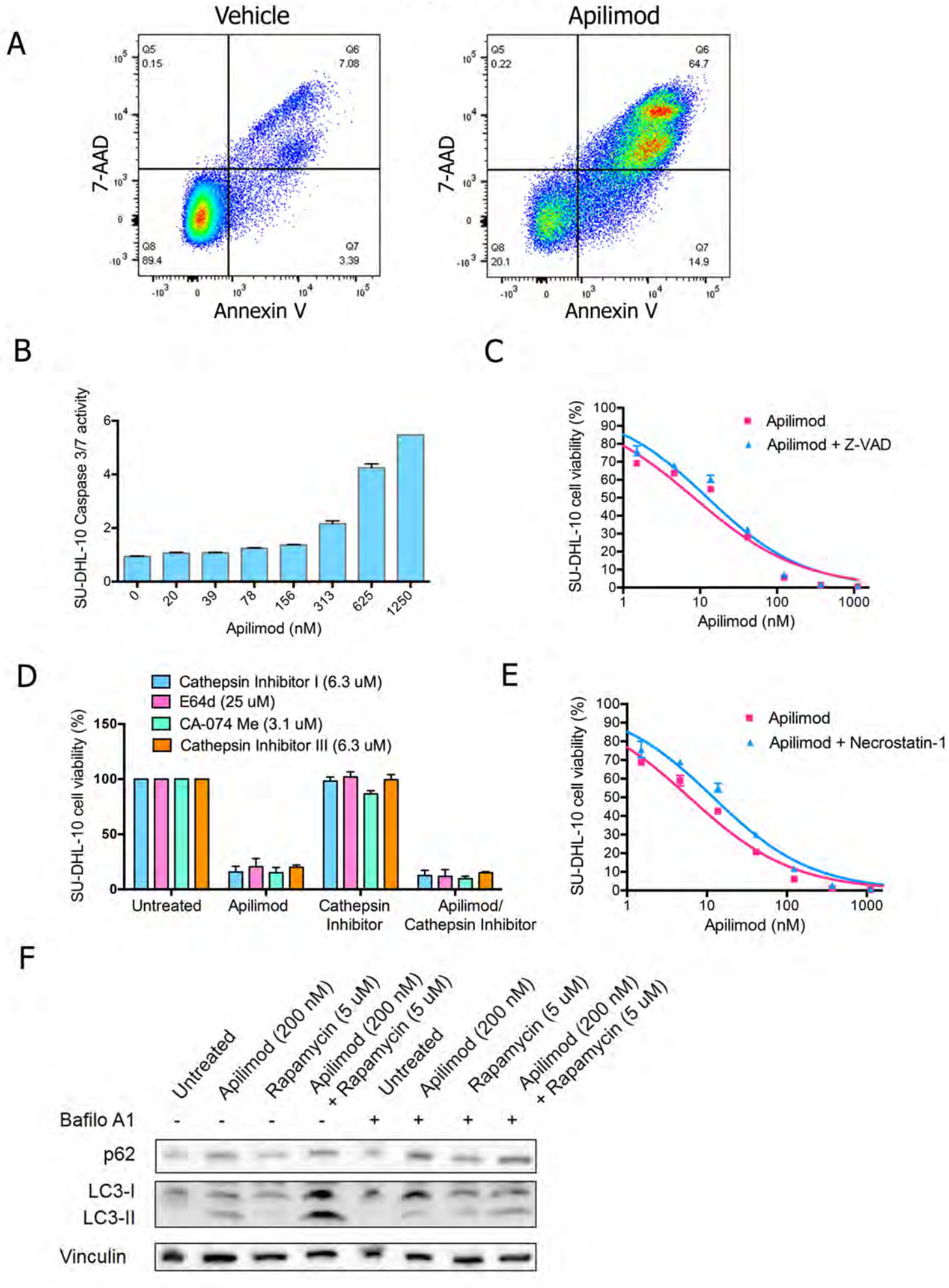
A
Vehicle
Apilimod
Q5
0.15
Q6
7.08
Q8
89.4
Q7
3.39
Q5
0.22
Q6
64.7
Q8
20.1
Q7
14.9
7-AAD
Annexin V
B
SU-DHL-10 Caspase 3/7 activity
0
20
39
78
156
313
625
1250
Apilimod (nM)
C
SU-DHL-10 cell viability (%)
Apilimod
Apilimod + Z-VAD
Apilimod (nM)
D
Cathepsin Inhibitor I (6.3 uM)
E64d (25 uM)
CA-074 Me (3.1 uM)
Cathepsin Inhibitor III (6.3 uM)
SU-DHL-10 cell viability (%)
Untreated
Apilimod
Cathepsin Inhibitor
Apilimod/ Cathepsin Inhibitor
E
SU-DHL-10 cell viability (%)
Apilimod
Apilimod + Necrostatin-1
Apilimod (nM)
F
Untreated
Apilimod (200 nM)
Rapamycin (5 uM)
Apilimod (200 nM) + Rapamycin (5 uM)
Bafilo A1
p62
LC3-I
LC3-II
Vinculin

Figure 4

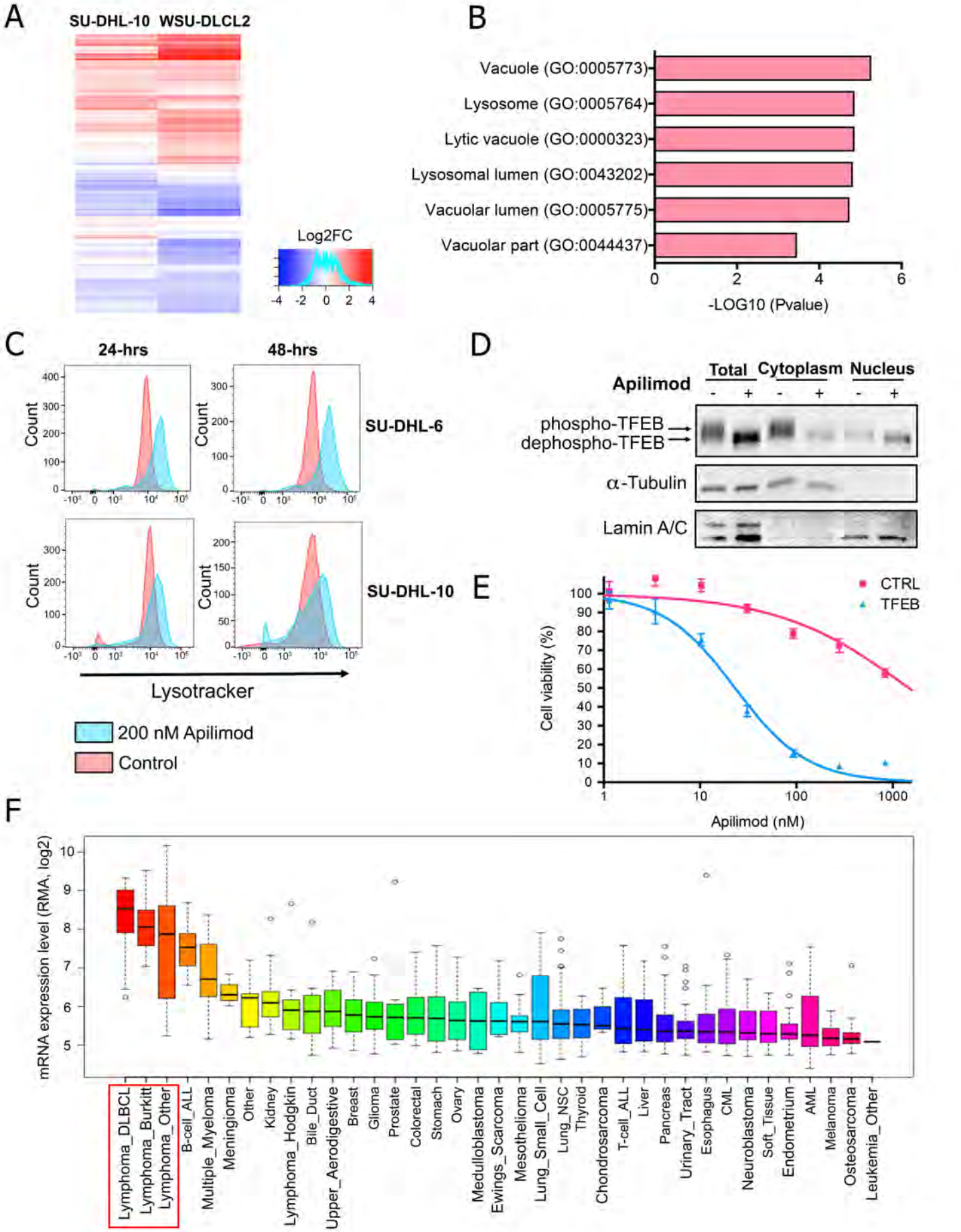
A
SU-DHL-10
WSU-DLCL2
Log2FC
-4 -2 0 2 4
B
Vacuole (GO:0005773)
Lysosome (GO:0005764)
Lytic vacuole (GO:0000323)
Lysosomal lumen (GO:0043202)
Vacuolar lumen (GO:0005775)
Vacuolar part (GO:0044437)
0 2 4 6
-LOG10 (Pvalue)
C
24-hrs
48-hrs
Count
SU-DHL-6
SU-DHL-10
Lysotracker
200 nM Apilimod
Control
D
Apilimod
Total
Cytoplasm
Nucleus
- + - + - +
phospho-TFEB
dephospho-TFEB
α-Tubulin
Lamin A/C
E
CTRL
TFEB
Cell viability (%)
Apilimod (nM)
F
mRNA expression level (RMA, log2)
Lymphoma_DLBCL
Lymphoma_Burkitt
Lymphoma_Other
B-cell_ALL
Multiple_Myeloma
Meningioma
Other
Kidney
Lymphoma_Hodgkin
Bile_Duct
Upper_Aerodigestive
Breast
Glioma
Prostate
Colorectal
Stomach
Ovary
Medulloblastoma
Ewings_Scarcoma
Mesothelioma
Lung_Small_Cell
Lung_NSC
Thyroid
Chondrosarcoma
T-cell_ALL
Liver
Pancreas
Urinary_Tract
Esophagus
CML
Neuroblastoma
Soft_Tissue
Endometrium
AML
Melanoma
Osteosarcoma
Leukemia_Other

Figure 5

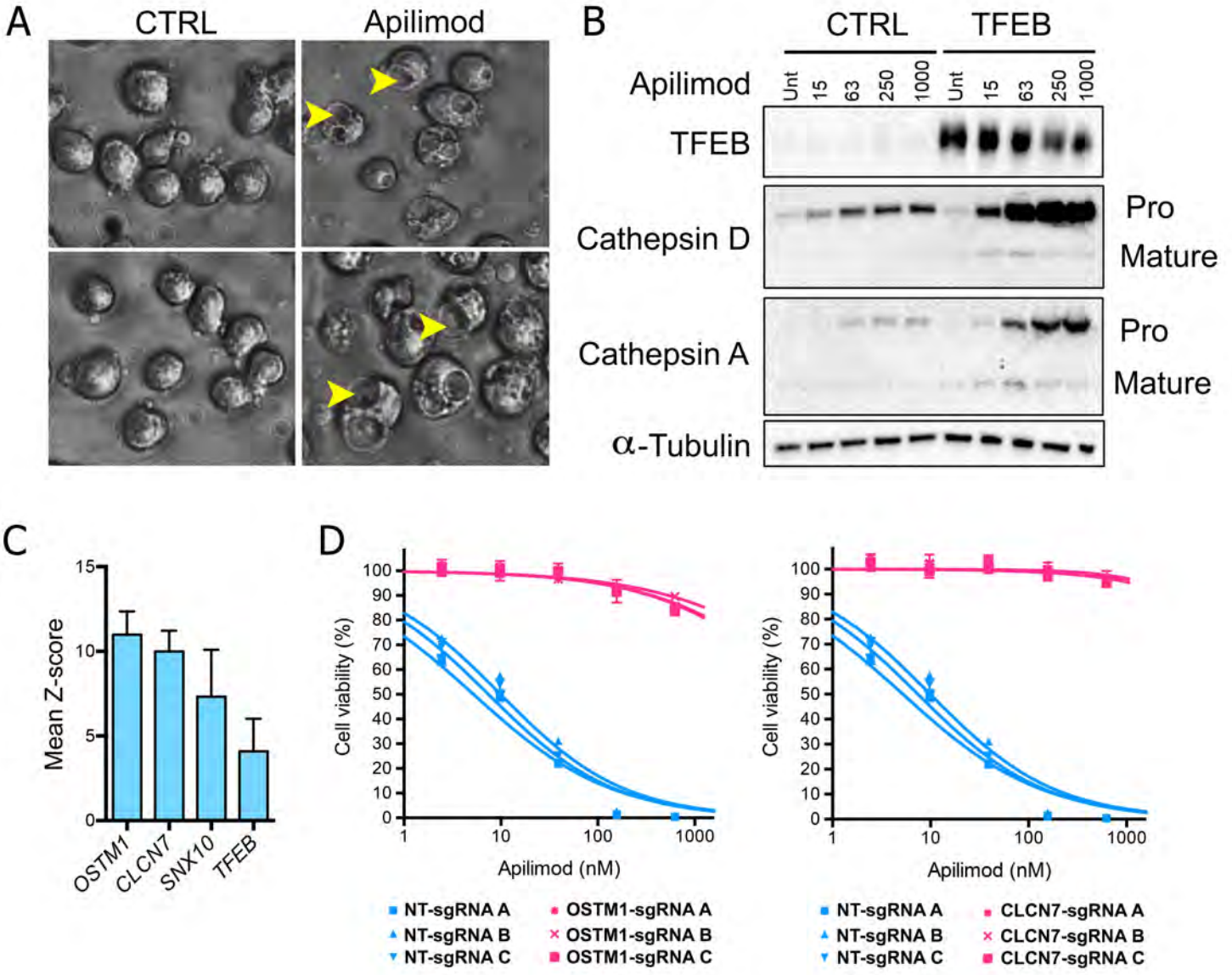
A
CTRL
Apilimod
B
CTRL
TFEB
Apilimod
Unt
15
63
250
1000
Unt
15
63
250
1000
TFEB
Cathepsin D
Pro
Mature
Cathepsin A
Pro
Mature
α-Tubulin
C
Mean Z-score
15
10
5
0
OSTM1
CLCN7
SNX10
TFEB
D
Cell viability (%)
Apilimod (nM)
NT-sgRNA A
NT-sgRNA B
NT-sgRNA C
OSTM1-sgRNA A
OSTM1-sgRNA B
OSTM1-sgRNA C
CLCN7-sgRNA A
CLCN7-sgRNA B
CLCN7-sgRNA C

Figure 6

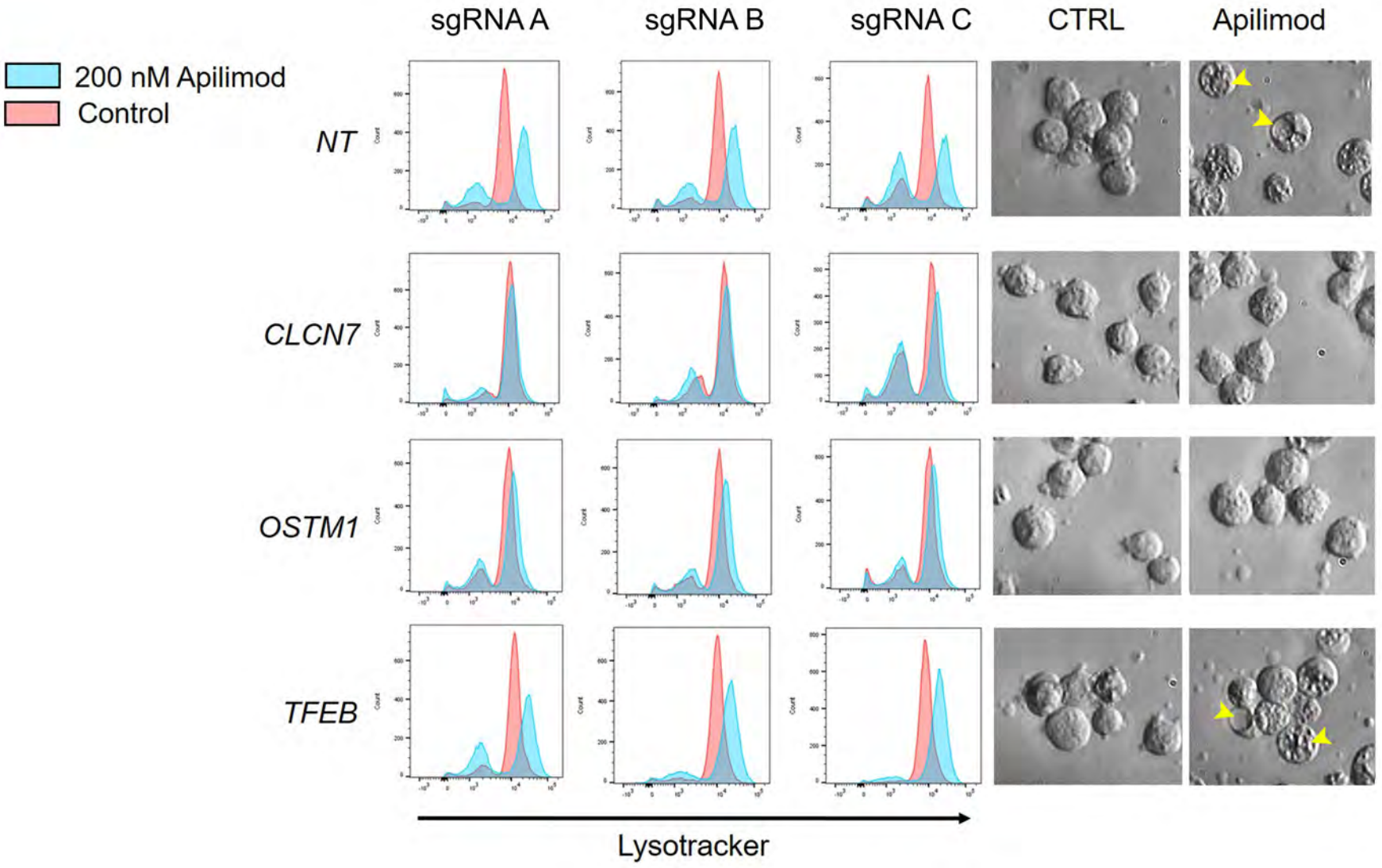
sgRNA A
sgRNA B
sgRNA C
CTRL
Apilimod
200 nM Apilimod
Control
NT
CLCN7
OSTM1
TFEB
Lysotracker

Identification of apilimod as a first-in-class PIKfyve kinase inhibitor for treatment of B-cell non-Hodgkin lymphoma

Sophia Gayle, Sean Landrette, Neil Beeharry, Chris Conrad, Marylens Hernandez, Paul Beckett, Shawn M. Ferguson, Talya Mandelkern, Meiling Zheng, Tian Xu, Jonathan Rothberg and Henri Lichenstein